

Scanning gate microscopy of current-annealed single layer graphene

M. R. Connolly¹, K. L. Chiou¹, C. G. Smith¹, D. Anderson¹, G.

A. C. Jones¹, A. Lombardo^{2,3}, A. Fasoli³, A. C. Ferrari³

¹*Cavendish Laboratory, Department of Physics,*

University of Cambridge, Cambridge, CB3 0HE, UK

²*DIEET, Universita' di Palermo, Italy and*

³*Department of Engineering, University of Cambridge, Cambridge, CB3 0FA, UK*

(Dated: July 4, 2021)

Abstract

We have used scanning gate microscopy to explore the local conductivity of a current-annealed graphene flake. Mapping the local neutrality point (NP) after annealing at low current density reveals micron-sized inhomogeneities which reflect the temperature distribution generated by ohmic heating. Broadening of the local e-h transition is also correlated with the spatial homogeneity of the NP. Annealing at higher current density improves the NP homogeneity, but we still observe some asymmetry in the e-h conduction. We attribute this to a hole doped region close to one of the metal contacts combined with underlying striations in the NP distribution.

PACS numbers:

Graphene exhibits a wealth of properties relevant to a wide range of applications and fundamental research.¹ To meet expectations and complement silicon in future nanoelectronics it is necessary to obtain precise and consistent control over its nanoscale electronic properties. Promising steps in this direction have been made using a combination of chemical functionalization and geometrical confinement.^{2,3,4,5,6} Developing techniques for analyzing and controlling the effect of these processes is thus at the forefront of graphene research. Scanning probes in particular have provided valuable insights into the substrate's influence on nanometer-scale topographic and potential fluctuations.^{7,8,9,10} At the mesoscale photocurrent^{11,12} and Raman^{13,14,15,16} microscopy have also been used to characterize doping from charged surface impurities and charge transfer from metal contacts. The presence of charged impurities manifests in the electrical transport as a shift in the charge neutrality point (NP),¹⁷ but the effect on the mobility and minimum conductivity at the NP is still debated.^{18,19} Mesoscopic (micron-sized) inhomogeneities in the impurity density also contribute to the random variations observed in the transport properties of as-prepared two terminal devices.²⁰ Annealing in an inert atmosphere and degassing reduces the NP shift and inhomogeneity,^{21,22} but unless a final cleaning step is performed *in situ* the improvement is limited due to the re-adsorption of atmospheric gases and water vapor.²² Current-annealing has been used for *in situ* removal of adsorbates,^{23,24} in many cases resulting in an electron-hole conduction asymmetry.^{2,23,25} Here, we use scanning gate microscopy (SGM)²⁶ to explore the local conductivity in a current-annealed graphene monolayer and show that persistent inhomogeneities in the remanent impurity density contribute to the anomalous e-h conduction. We investigate a graphene flake ($\sim 8 \times 8 \mu\text{m}^2$) mechanically exfoliated from natural graphite onto a highly doped Si substrate capped with a 300 nm thick SiO₂ layer. Optical microscopy²⁷ and Raman spectroscopy²⁸ were used to locate the flake and confirm that it is a monolayer. Two 50 nm thick Au contacts were patterned using e-beam lithography and lift-off processing [see inset of Fig. 1(a).] The sample was annealed at 200°C in N₂/H₂(5%) to remove resist residue and mounted to the head of a scanning probe microscope evacuated to 10⁻⁵ mbar. Further cleaning was performed *in situ* by driving $J \approx 5 \times 10^8 \text{ A/cm}^2$ through the device and monitoring the shift in the neutrality point voltage (V_{NP}).²³ The two terminal resistance R as a function of voltage V_{BG} applied to the Si back-gate [Fig. 1(a)] reveals shifts of $\approx 3 \text{ V}$ in V_{NP} every 10 minutes. We assume the initial $V_{NP} \approx 25 \text{ V}$ is due to hole-doping adsorbates such as H₂O and O₂. Using $n = \alpha(V_{BG} - V_{NP})$ ($\alpha = 7.2 \times 10^{10}$

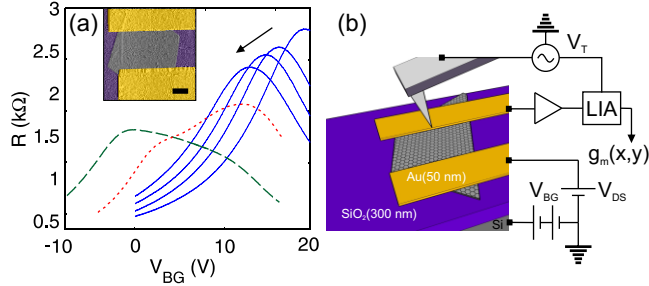


FIG. 1: (a) $R(V_{BG})$ measured at 10 min intervals (blue, solid) (arrow indicates the direction of shift in peak position,) and after 9 hours (red, dotted) of current annealing at $J \approx 5 \times 10^8$ A/cm². After 10 mins at $J \approx 1 \times 10^9$ A/cm² (green, dashed). Inset: False-color atomic force micrograph of the sample (scale bar 2 μ m). (b) Schematic of the setup used to perform SGM.

cm⁻²)¹⁷ to estimate the carrier density, we obtain a mobility of ≈ 8000 cm²V⁻¹s⁻¹ at $n \approx 2 \times 10^{11}$ cm⁻². The final cleaning current was applied for ≈ 9 hours, resulting in a shift in the bulk V_{NP} from ≈ 25 V to ≈ 16 V [red curve, Fig. 1(a)], and a pronounced shoulder appearing at $V_{BG}=6$ V. The latter is characteristic of flakes divided into regions with different carrier density, either by chemical doping,^{21,29} or invasive metal contacts.²⁰ The suppression of R is also typical of flakes with a mesoscopic NP inhomogeneity.²⁰ Our SGM setup is shown in Fig. 1(b) (see Ref.[26] for details.) To benefit from the high signal-to-noise ratio achievable using a.c. detection, we modulate the potential difference V_T between the tip (Pt/Ir coated NanoWorld ARROW-NCpt) and the graphene at low frequency (typically 3 V @ 1 kHz) and detect the modulation of I_{DS} (≈ 250 μ A) using a lock-in amplifier. We quantify the demodulated component ($\delta I_{DS} \approx 0.1$ μ A) by the local transconductance $g_m = \partial I_{DS} / \partial V_T$ normalized to the bulk conductance $G(V_{BG})$.²⁶

Figure 2(a) plots $g_m(V_{BG})$ measured with the tip in each of the regions indicated in the diagram of the device (inset, Fig. 2.) G is suppressed ($g_m < 0$) at each tip position when $V_{BG} < 6$ V. The opposite is true for $V_{BG} > 16$ V, when G is everywhere enhanced ($g_m > 0$). The crossover back-gate voltage $V_0 = V_{BG}(g_m=0)$ falls within the range of intermediate V_{BG} and shows a sensitive dependence on tip position. To understand the basic form of the measured $g_m(V_{BG})$, we relate the conductivity σ_L of the $\approx (50$ nm)² region perturbed by the tip¹⁰ to a local carrier density by $\sigma_L(x, y) = |\alpha V_{BG} + \beta V_T + \bar{n}| e \mu$, where β is the capacitive coupling between the tip and graphene, and \bar{n} is the local impurity-induced charge

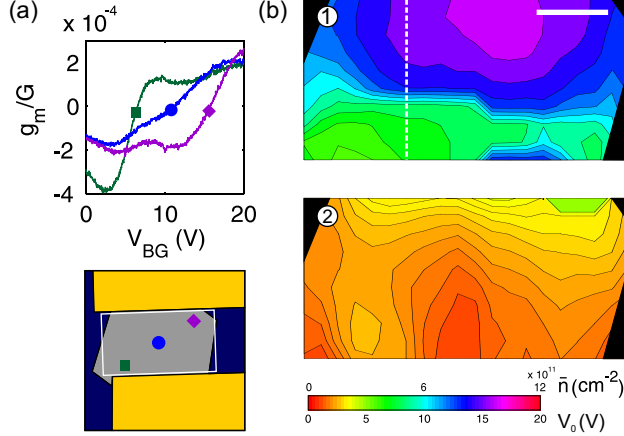


FIG. 2: (a) Normalised transconductance measured with the tip at the locations marked in the inset. (b) Contour plot of the neutrality point V_0 of the flake in the states corresponding to the red (1) and green (2) back-gate sweeps in Fig.1(a) (Scale bar $2 \mu\text{m}$.)

density.^{19,30,31} Neglecting quantum contributions to the conductivity, g_m is proportional to $\partial\sigma_L(x,y)/\partial V_T$, which changes sign at the local NP when $V_{BG} = V_0 \approx \bar{n}(x,y)/\alpha$ (since $\langle V_T \rangle = 0$). Hence V_0 is a measure of \bar{n} , which can be empirically related to the impurity density n_i via $\bar{n} \propto n_i^b$ ($b = 1.2-1.3$).¹⁹ We explore $\bar{n}(x,y)$ by measuring $g_m(V_{BG})$ with the tip positioned over a grid of points with pitch ≈ 300 nm and constructing the map of $\alpha V_0(x,y)$ shown in panel 1 of Fig. 2(b). A band with $\bar{n} \approx 4.3 \times 10^{11} \text{ cm}^{-2}$ (6 V) runs across the flake parallel to the contacts, asymmetrically flanked by regions with higher density close to the contacts, where $\bar{n} \approx 11 \times 10^{11} \text{ cm}^{-2}$ (16 V). This \bar{n} profile can be explained by assuming that it reflects the temperature distribution generated by ohmic heating during current annealing. The remanent \bar{n} distribution in this case suggests that energy is dissipated in the flake itself, while the contacts act as heat sinks. A similar temperature distribution was inferred from previous scanning probe²³ and Raman³² microscopy measurements, though here the asymmetry either side of the higher temperature region is more pronounced. The two values of V_0 also coincide with the positions of the shoulder and the maximum of the bulk $R(V_{BG})$ [red curve, Fig. 1(a)], confirming that these features originate from the mesoscopic inhomogeneity. Figure 3(a) shows plots of the local conductivity $\sigma_L(V_{BG})$ reconstructed by numerically integrating $g_m(V_{BG})$ [Fig. 2(a)]. Within the framework of Ref. [30], the width of the minimum conductivity plateau ΔV_{BG} at the NP is expected to increase with \bar{n} .^{19,30} While we did not observe this direct relationship, Fig. 3(b) reveals a linear correlation between

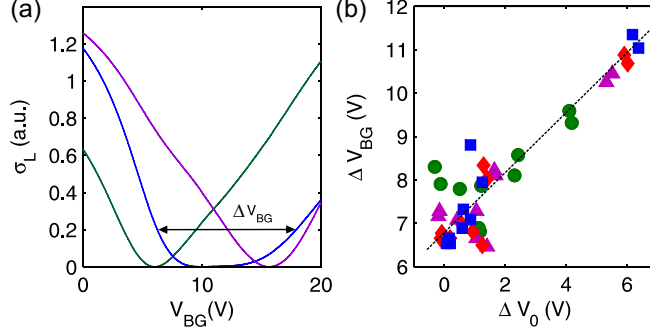


FIG. 3: (a) Local conductivity at the same locations marked in Fig. 2(b) (reconstructed by integrating $g_m(V_{BG})$.) Each curve has been vertically offset such that $\sigma_L(V_0)=0$. Correlation plots between ΔV_{BG} and ΔV_0 , the change in V_0 along linescans in the vicinity of the dashed line in Fig. 2(b). Dashed line is drawn to indicate the linear trend.

ΔV_{BG} and the spatial gradient of V_0 along parallel lines in the vicinity of the dashed line in Fig. 2(b). (We extract ΔV_{BG} for each curve by subtracting the back-gate voltages where $\sigma_L \approx 0.2$.) This is understandable as broadening is most pronounced when the tip gates both n - and p -type regions, in the same way that ΔV_{BG} in homogeneous flakes is broadened by e-h puddles at low carrier density.³⁰

To assess the inhomogeneity remaining when $V_{NP} \approx 0$, we annealed the flake at $J \approx 1 \times 10^9$ A/cm² for 10 minutes and repeated the measurement of $\bar{n}(x, y)$. The resulting \bar{n} map is shown in panel 2 of Fig. 2(b) and the corresponding $R(V_{BG})$ sweep in Fig. 1(a)(green curve). In line with the previous analysis, the single peak in $R(V_{BG})$ coincides with the average value of V_0 (≈ 2 V) ($\bar{n} = 1 \times 10^{11}$ cm⁻²), and the greater homogeneity is reflected by the absence of the shoulder. However, upon close inspection we observe a region close to the top contact with $\bar{n} = 7 \times 10^{11}$ cm⁻². The doping in this region, which persisted even after annealing with $J > 1 \times 10^9$ A/cm², is responsible for the remaining asymmetry in $R(V_{BG})$, since opposing changes in R occur in regions with opposite carrier type.²⁰ Figure 4(a) shows a raw $g_m(x, y)$ ($V_{BG} = 3$ V) image of the flake after the second current anneal [c.f. green curve, Fig. 1(a)]. Such images provide complementary information to the maps of $\bar{n}(x, y)$ by allowing one to resolve finer \bar{n} variations directly via changes in g_m . Superimposed on the micron-sized inhomogeneity are pronounced striations in g_m that span the length of the flake with lateral period of ≈ 100 nm (see linescan, Fig. 4(b)). These modulations could be caused by enhanced heating from resistive hotspots in the disordered pn junctions formed

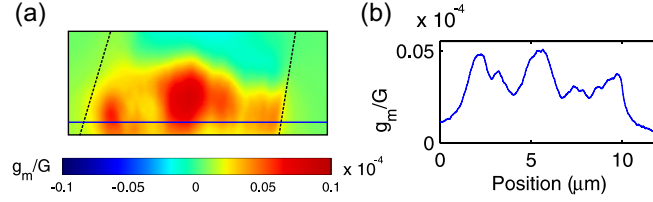


FIG. 4: (a) SGM image ($12\ \mu\text{m} \times 5\ \mu\text{m}$) mapping g_m at $V_{BG} = 3\ \text{V}$ [c.f. green curve, Fig. 1(a)]. (b) Profile of g_m along the line in image (a).

close to the metal-graphene interface,²⁰ or electromigration of material from the contacts.²³ By inspecting the amplitude of the modulation in g_m , we estimate that these striations reflect an impurity density fluctuation $\Delta\bar{n} \sim 7.2 \times 10^9\ \text{cm}^{-2}$, which may impose an intrinsic limit to the homogeneity achievable when current annealing supported flakes.

In conclusion, SGM is a powerful method for characterizing the local conductivity of inhomogeneously doped graphene. We find that the local NP reflects the temperature distribution generated by ohmic heating and also exhibits finer linearly correlated inhomogeneities. Both types of inhomogeneity are likely to contribute to the e-h asymmetry observed in current-annealed flakes.

This work was financially supported by the European GRAND project (ICT/FET). ACF acknowledges funding from the European Research Grant NANOPOTS and the Royal Society.

¹ A. K. Geim and K. S. Novoselov, *Nature Materials* **6**, 183 (2007).

² X. Wang, X. Li, L. Zhang, Y. Yoon, P. K. Weber, H. Wang, and H. Dai, *Science* **324**, 768 (2009).

³ M. Y. Han, B. Ozyilmaz, Y. Zhang, and P. Kim, *Phys. Rev. Lett* **98**, 206805 (2007).

⁴ B. Ozyilmaz, P. Jarillo-Herrero, D. Efetov, and P. Kim, *Appl. Phys. Lett.* **91**, 192107 (2007).

⁵ F. Cervantes-Sodi, G. Csanyi, S. Piscanec, and A. C. Ferrari, *Phys. Rev. B* **77**, 165427 (2008).

⁶ Z. Chen, Y.-M. Lin, M. J. Rooks, and P. Avouris, *Physica E* **40**, 228 (2009).

⁷ A. Deshpande, W. Bao, F. Miao, C. N. Lau, and B. J. LeRoy, *Phys. Rev. B* **79**, 205411 (2009).

⁸ J. Martin, N. Akerman, G. Ulbricht, T. Lohmann, J. Smet, K. V. Klitzing, and A. Yacoby, *Nature physics* **4**, 144 (2008).

- ⁹ Y. Zhang, V. W. Brar, C. Girit, A. Zettl, and M. F. Crommie, *Nature Physics* **5**, 722 (2009).
- ¹⁰ J. Berezovsky and R. M. Westervelt, arXiv:0907.0428v1 (2009).
- ¹¹ E. J. H. Lee, K. Balusubramanian, R. T. Weitz, M. Burghard, and K. Kern, *Nature Nanotechnology* **3**, 486 (2008).
- ¹² T. Mueller, F. Xia, M. Freitag, J. Tsang, and P. Avouris, *Phys. Rev. B.* **79**, 245430 (2009).
- ¹³ Y.-J. Yu, Y. Zhao, S. Ryu, L. E. Brus, K. S. Kim, and P. Kim, *Nano Lett.* **9**, 3430 (2009).
- ¹⁴ C. Casiraghi, S. Pisana, K. S. Novoselov, A. K. Geim, and A. C. Ferrari, *Appl. Phys. Lett.* **91**, 233108 (2007).
- ¹⁵ C. Stampfer, F. Molitor, D. Graf, K. Ensslin, A. Jungen, C. Hierold, and L. Wirtz, *Appl. Phys. Lett.* **91**, 241907 (2007).
- ¹⁶ A. Das, S. Pisana, S. Piscanec, B. Chakraborty, S. K. Saha, U. V. Waghmare, R. Wang, H. R. Krishnamurthy, A. K. Geim, A. C. Ferrari, et al., *Nature Nano.* **3**, 210 (2008).
- ¹⁷ K. S. Novoselov, A. K. Geim, S. V. Morozov, D. Jiang, Y. Zhang, S. V. Dubonos, I. V. Grigorieva, and A. A. Firsov, *Science* **306**, 666 (2004).
- ¹⁸ L. A. Ponomarenko, R. Yang, T. M. Mohiuddin, M. I. Katsnelson, K. S. Novoselov, S. V. Morozov, A. A. Zhukov, F. Schedin, E. W. Hill, and A. K. Geim, *Phys. Rev. Lett* **102**, 206603 (2009).
- ¹⁹ J. H. Chen, C. Jang, M. Ishigami, S. Xiao, W. G. Cullen, E. D. Williams, and M. S. Fuhrer, *Solid State Communications* **149**, 1080 (2009).
- ²⁰ P. Blake, R. Wang, S. V. Morozov, F. Schedin, L. A. Ponomarenko, A. A. Zhukov, R. R. Nair, I. V. Grigorieva, K. S. Novoselov, and A. K. Geim, *Solid State Communications* **149**, 1068 (2009).
- ²¹ T. Lohmann, K. von Klitzing, and J. H. Smet, *Nano Lett.* **9**, 1973 (2009).
- ²² H. E. Romero, N. Shen, P. Joshi, H. R. Gutierrez, S. A. Tadigadapa, J. O. Sofo, and P. C. Eklund, *ACS Nano* **2**, 2037 (2008).
- ²³ J. Moser, A. Barrierro, and A. Bachtold, *Appl. Phys. Lett.* **91**, 163513 (2007).
- ²⁴ K. I. Bolotin, K. J. Sikes, Z. Jiang, M. Klima, G. Fudenberg, J. Hone, P. Kim, and H. L. Stormer, *Solid State Communications* **146**, 351 (2008).
- ²⁵ X. Du, I. Skachko, F. Duerr, A. Luican, and E. Y. Andrei, *Nature* **462**, 192 (2009).
- ²⁶ R. Crook, C. G. Smith, C. G. Simmons, and D. A. Ritchie, *J. Phys.: Condens. Matt.* **12**, L375 (2000).

- ²⁷ C. Casiraghi, A. Hartschuh, E. Lidorikis, H. Qian, H. Harutyunyan, T. Gokus, K. S. Novoselov, and A. C. Ferrari, *Nano Lett.* **7**, 2711 (2007).
- ²⁸ A. C. Ferrari, J. C. Meyer, V. Scardaci, C. Casiraghi, M. Lazzeri, F. Mauri, S. Piscanec, D. Jiang, K. Novoselov, S. Roth, et al., *Phys. Rev. Lett* **97**, 187401 (2006).
- ²⁹ D. B. Farmer, Y.-M. Lin, A. Afzali-Ardakani, and P. Avouris, *Appl. Phys. Lett.* **94**, 213106 (2009).
- ³⁰ S. Adam, E. H. Hwang, V. M. Galitski, and S. D. Sarma, *PNAS* **104**, 18392 (2007).
- ³¹ E. Rossi, S. Adam, and S. D. Sarma, *Phys. Rev. B* **79**, 245423 (2009).
- ³² M. Freitag, M. Steiner, Y. Martin, V. Perebeinos, Z. Chen, J. C. Tsang, and P. Avouris, *Nano Lett.* **9**, 1883 (2009).